Design and testing of a microfluidic biochip for cytokine enzyme-linked immunosorbent assay

Hongyan He,[1,2] Yuan Yuan,[1] Weixiong Wang,[1] Nan-Rong Chiou,[3] Arthur J. Epstein,[4] and L. James Lee[1,5,a)]

[1]*Nanoscale Science and Engineering Center for Affordable Nanoengineering of Polymeric Biomedical Devices, The Ohio State University, Columbus, Ohio 43210, USA*
[2]*BioLOC, LLC, 1381 Kinnear Road Suite 100, Columbus, Ohio 43212, USA*
[3]*Nanomaterial Innovation Ltd., 3390 Green River Dr., Columbus, Ohio 43228, USA*
[4]*Department of Physics, The Ohio State University, Columbus, Ohio 43210, USA*
[5]*Department of Chemical and Biomolecular Engineering, The Ohio State University, Columbus, Ohio 43210, USA*

(Received 20 February 2009; accepted 16 March 2009; published online 13 April 2009)

Enzyme-linked immunosorbent assay (ELISA) has been widely used in medical diagnostics, environmental analyses, and biochemical studies. To reduce assay time and lower consumption of reagents in cytokine ELISA analysis, a polymeric microfluidic biochip has been designed and fabricated via several new techniques: Polyaniline-based surface modification for superhydrophobic capillary valving and oxygen plasma-poly(ethyleneimine)-tyrosinase-protein A modification for high sensitivity protein detection. The proper flow sequencing was achieved using the superhydrophobic capillary valves. The burst frequency of each valve was experimentally determined and compared with two capillary force equations and the fluent finite element simulation. This fully automated microfluidic biochip with an analyzer is able to provide high fluorescence signal of ELISA with a wider linear detection range and a much shorter assay time than 96-well microtiter plates. It is applicable to a variety of nonclinic research and clinically relevant disease conditions. The modification technologies in this study can be implemented in other lab-on-a-chip systems, drug/gene delivery carriers, and other immunoassay biosensor applications. © *2009 American Institute of Physics.* [DOI: 10.1063/1.3116665]

I. INTRODUCTION

Enzyme-linked immunosorbent assay (ELISA), one of the most common immunoassays, is widely used for detection and quantification of chemical and biological molecules (antigens, mainly proteins and polypeptides) and is becoming more important in clinical diagnostics, food safety testing, and environmental monitoring. This technology is applicable to a variety of clinically relevant diseases, including melanoma,[1] breast cancer,[2] human immunodeficiency (HIV) detection,[3] liver diseases,[4] and many other medical conditions where prognosis/diagnosis/monitoring therapy relies on quantification from an ELISA. Conventional ELISA is tedious and laborious with a protocol involving a series of mixing, incubation, and washing steps typically carried out in a 96-well microtiter plate. Figure 1 illustrates the general principle and procedures of ELISA used in a 96-well microtiter plate.[5] In general, a primary antibody against the antigen (analyte) to be detected must be adsorbed onto a solid surface (step 1). After incubation, the unbounded antibodies are washed away. Blocking agents (usually proteins) are then added to block all the remaining binding sites on the solid surface to eliminate the nonspecific binding of proteins or antibodies (step 2). Samples or standards containing antigens are then introduced and

a)Author to whom correspondence should be addressed. Electronic mail: leelj@chbmeng.ohio-state.edu. Tel.: (614) 292-2408. FAX: (614) 292-3769.

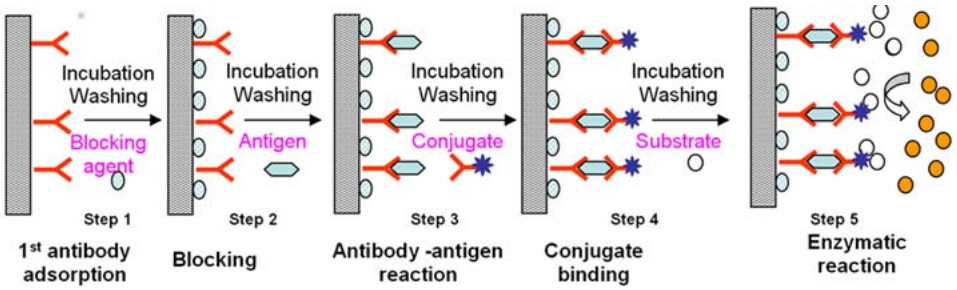

FIG. 1. The general principle and procedures of sandwich-type ELISA.

incubated for sufficient time to allow the immunoreaction between the primary antibodies and the antigens to take place (step 3). The enzyme-linked secondary antibodies (conjugates) are then added to bind with antigens (step 4). After incubation, the excess conjugates are washed away. Finally, the enzyme substrates are introduced and converted into products with a detectable signal (e.g., color or fluorescence) (step 5). The results often have large errors and/or inconsistencies. Each assay involves the use of expensive antibodies and reagents and usually takes several hours or longer because of the long incubation time required in each step.[6] To overcome these drawbacks, several microfluidic ELISA devices have been developed on the surfaces of a single microchannel or using microbeads trapped in a microchannel.[7–9] With a high surface to volume ratio of the microchannel, these assays demonstrated the potential for fast immunoreaction assay times compared to the usual microtiter 96-well plate ELISA. However, each step of the ELISA in all of these assays was still carried out manually.

The centrifugal fluidic platform technology was first developed in 1969,[10] and the concept since then has been extensively studied.[11–14] A recent review of compact disk (CD)-based microfluidic platform technology and its applications can be found in the literature.[15] The CD platform has been commercialized for high throughput screening by Tecan, Gyros AB, Abaxis system, and Burstein Technologies. Although CD microfluidics is a technology that has been demonstrated successfully by these companies, it has been seldom applied to complicated immunoassays such as the sandwich-type ELISA. The only commercially available system is GyroLab Workstation which delivers high-quality and reliable results and offers significant advantages over the conventional microplate methods.[16] However, the use of an expensive robotic system for multiple reagent loading and expensive streptavidin-coated microbeads in the detection area severely limits its applications. There is a great need of a fully automated low-cost ELISA system that is fast and easy to use, uses small amount of reagents and sample, and requires minimum manual labor, thus reducing the associated handling errors without the need of a robotic unit.

Combining microfluidic immunoassay with centrifugal fluidic technology, our group has developed a novel CD-ELISA platform. The CD-ELISA is a self-contained microdevice that incorporates low-power microfluidic components and high-sensitivity immunomolecules, and is capable of performing parallel and multiple tests with high precision. The CD platform integrates a number of microfluidic functions. These include pumping, capillary valve control, fluid splitter, washing, and mixing with required antibodies, reagents, and buffer solution in distinctly placed reservoirs. By spinning the disk, the centrifugal force overcomes the capillary force in the valves, and the fluid in each reservoir is released sequentially replacing the stepwise procedures carried out in the conventional ELISA process. However, as a new technology, developing a CD-ELISA faces significant challenges. These involve the development of functioning valves to control the sequence of fluid/reagent flow for each step of the ELISA assay, efficient antibody binding, and a CD-ELISA analyzer.

Based on the requirement of energy to operate, the microfluidic valves can be divided into two groups: Passive valves without energy requirement[17,18] and active valves that need energy input to perform their action.[19–21] Among all microvalves, the capillary valve is the simplest and can be implemented easily into the microfluidic design and fabrication. Capillary valving has the advan-

tage of not requiring any moving parts and external actuation. Recently, this type of valve has attracted a great deal of attention for applications in various microfluidic systems.[22,23] For pure water or buffer solutions, the capillary valve works well because a proper hydrophobic polymer surface can be chosen to provide a desirable contact angle. However, proteins exist in the solutions used in ELISA. The phenomena of protein adsorption onto plastic substrates have been widely observed. Due to protein adsorption, the surface of the capillary valve gradually becomes hydrophilic and the solution would wick through, leading to the failure of the valving function. The issue becomes more serious, i.e., the capillary valve cannot even hold the solutions in the reservoirs, when the blocking solution (protein) is applied on the microchannels to prevent nonspecific binding of proteins. One way to overcome this problem is to implement a superhydrophobic coating in the valve areas. There are various methods to create superhydrophobic surfaces.[24–30] We use polyaniline nanofibers along with the noncrystalline fluorine coating to create nanostructures in the capillary valves. "Hierarchical roughness" of nanosized papillae makes the valve surfaces superhydrophobic and much less affected by protein binding.

Another major challenge for microscale biodevices is the low detection sensitivity because of very low reagent volume (1%–3% that of the 96-well microtiter plates). The antibody commonly immobilized on biochips by the conventional passive adsorption only results in a few functional sites, leading to a limited dynamic linear range, low signal-to-noise ratio, and low detection sensitivity. To overcome this problem, several antibody-polymer immobilization strategies have been developed to improve the antibody binding ranging from antibody passive adsorption or covalent immobilization on microbead/gel,[31–33] covalent crosslink via linkage reagents,[34–36] to covalent immobilization by polymer linker.[37] However, these methods either need special manipulation devices[31,33] or involve several intermediates and environmentally unfriendly solvents.[34–36] Furthermore, the antibody molecules immobilized using these strategies are all randomly absorbed in a mixed prone-upright state on the substrate, resulting in a great reduction in the activity of antibody to bind antigen. Therefore, there is a great need to develop a facile and efficient method to enhance the sensitivity of ELISA in the polymeric microfluidic devices. "Y" shaped immunoglobulin G (IgG) consists of one F_c and two F_{ab} fragments. The proper orientation of antibodies can yield higher antigen-binding capacity and consequently higher sensitivity than randomly oriented antibodies.[38–40] Among many approaches for orientation-controlled immobilization of antibodies, the use of binding protein A appears to be most attractive as it enables a more favorable orientation of antibodies than adsorption, covalent binding, or cross linking.[41,42] Although, protein A has been used extensively to immobilize target proteins, it has not been utilized for microchip-based ELISA applications.

In this study, a microfluidic compact disk with splitters for multiple samples was precisely designed and manufactured. A capillary valve modified with polyaniline nanofibers was applied to manipulate fluids and provide proper flow sequencing. A tyrosinase (TR) catalyzed protein A strategy was applied to immobilize antibody for enhanced sensitivity of ELISA immunoassay. The ELISA for detecting interferon-gamma (IFN-γ) was carried out on this microfluidic system to demonstrate the applicability of CD-ELISA for detecting biomedical samples.

II. EXPERIMENTAL

A. Materials and reagents

Aniline, ammonium peroxydisulfate (APS), poly(ethyleneimine) (PEI) (MW 75 000), protein A from Staphylococcus aureus, TR (25 U.K.), and 3-*p*-hydroxyphenylpropionic acid (HPPA) were all purchased from Sigma Chemical (St. Louis, MO). Aniline was distilled under vacuum before use and APS was used directly as received without further purification. The dopant acids, perchloric acid (HClO4), were used to study the formation of polyaniline nanofibers in the dilute polymerization.[43] The huIFN-γ coating mAb (anti-IFN-γ), biotinylated huIFN-γ detection mAb, and recombinant huIFN-γ cytokine (IFN-γ) were the primary antibody, the second antibody, and the detected "analyte" or antigen used in this study. They were purchased from Pierce Biotechnology (Rockford, IL) and reconstituted in distilled water and stored at −80 °C until use. Horse-

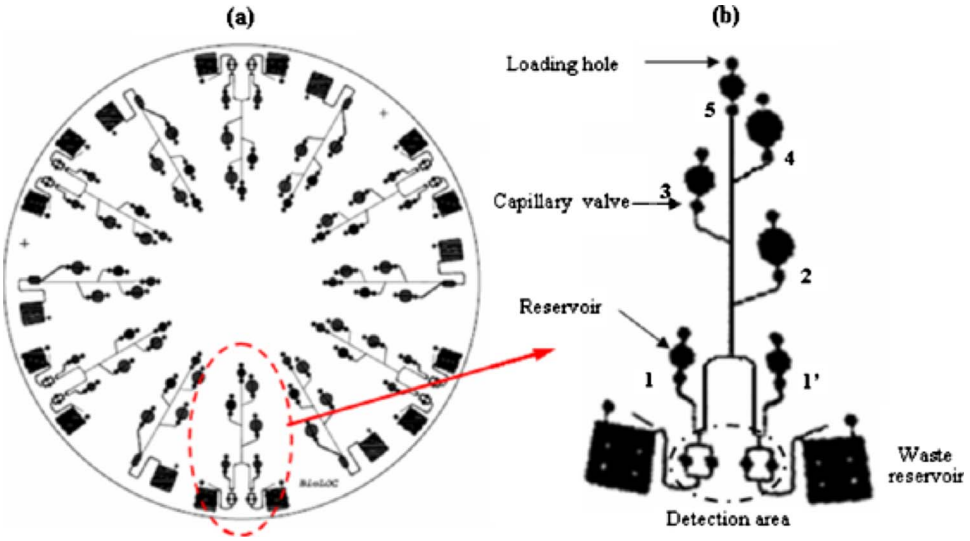

FIG. 2. Computer-aided design of (a) a 12-set compact disk with capillary valves and splitters and (b) a single assay on the compact disk. The primary antibody was preimmobilized at the detection area. The mixture of antigen and second antibody was loaded in reservoirs 1 and 1′. Reservoirs 2 and 4 were used for washing solution. Reservoirs 3 and 5 were used for conjugate and substrate, respectively.

radish peroxidase (HRP)-conjugated streptavidin and EZ-Label™ rhodamine protein labeling kit were also purchased from Pierce Biotechnology. Polyoxyethylenesorbitan monolaurate (Tween-20) was purchased from Bio-Rad Laboratories (Hercules, CA). Poly(methyl methacrylate) (PMMA) plates and chips were provided by RITEK in Taiwan. The microchannels and reservoirs on the chips are all 200 μm in depth. They are stored in a vacuum oven at 60 °C for at least 24 h before use. Bovine serum albumin (BSA) (Grand Island, NY) was purchased from Invitrogen Corporation. BSA solutions in de-ionized (DI) water were prepared with a concentration of 1.0 wt % as the blocking solution. Food dye was purchased from McCormick & Co., Inc. (Hunt Valley, MD). To evaluate the valve function, 0.1 wt % BSA solution was used for demonstration and a very small amount of food dye was added in the BSA solution to facilitate observation. All reagents, unless specified, were of analytical grade and were used without further purification.

B. Compact disk design and fabrication

A multiple-sample assay design on a 12 cm disk is shown in Fig. 2(a) and the schematic of a single design is given in Fig. 2(b). The designed chips and the cover lids were produced by a world-leading CD producer, RITEK, using PMMA as the material and microinjection molding as the manufacturing process. In the process, the injection molding was conducted on a high-speed injection machine (Sumitomo SD-35E). First, a stamper with microfluidic patterns was mounted onto the mold of injection machine and ready for injection molding. With the appropriate injection parameters adjusted, the plastic disk substrates were fabricated and then picked up from the injection machine. After that, the replicated chips were put onto a rotating stage for cooling. This low cost and mass-produced protocol has been used to make the prototype chips for our applications shown in Fig. 3. The primary antibody and blocking protein were preimmobilized onto the detection area. Then the substrate, conjugate, washing, second antibody, and antigen solution (i.e., sample) were loaded into corresponding reservoirs for flow sequencing and ELISA testing. Centrifugal and the capillary forces are used to control the flow sequence of different solutions involved in the ELISA process. In this five-reservoir ELISA process, only the composition of unknown sample (i.e., antigen) is different, while all other reagents used in the assay have the same composition. Therefore, one splitter is designed for reservoirs 1 and 1′, each of which is used for loading two individual samples (antigens). The splitters for the detection area shown in

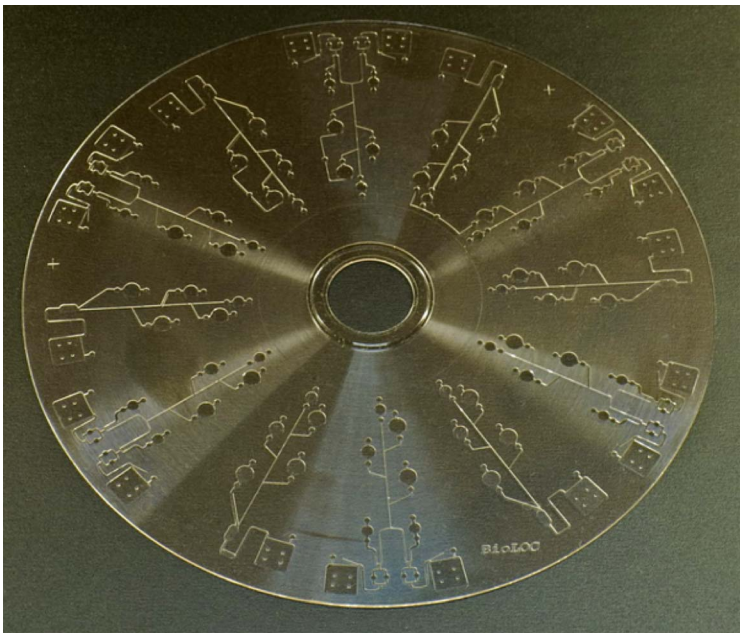

FIG. 3. An injection-molded compact disk ELISA chip.

Fig. 2(b) are designed for sample duplication. The patterns shown in Fig. 2(a) involve two types of patterns: With or without the splitters. This "model chip" design allows comparison and testing of splitters on a single CD. Ideally, the splitters in this new design will increase the 12 sets on a CD-ELISA chip to provide the capability to analyze 24 samples in duplicate providing 48-sample assay analysis.

C. Design of capillary valves

The valves we used are termed "capillary burst valves." When the centrifugal force of the spinning CD is greater than the opposing capillary force (the burst frequency), the liquid in the reservoir bursts through the valve and the liquid flows to the optode. At the connection of the reservoir exit channel and valve (or junction), there exists the juxtaposition of two opposing forces (shown in Fig. 4). The first one is the capillary force resulting from the surface tension in the junction where the microchannel meets the valve. When the fluid comes to the junction through the microchannel, the capillary force at the end of the microchannel tends to hold the fluid due to geometry change. The capillary force per unit area (P_s) is given by

$$\Delta Ps = \frac{C\gamma \sin\theta}{A}, \tag{1}$$

where γ is the surface tension of the fluid, θ is the contact angle, A is the cross-section area of the microchannel, and C is the associated contact line length. The opposing force ΔP_c results from the centrifugal force generated from the rotation of the disk. This force can be calculated from the following equation:

$$\Delta P_C = \rho\omega^2(R_2 - R_1)\left(\frac{R_1 + R_2}{2}\right) = \rho\omega^2 \cdot \Delta R \cdot \bar{R}, \tag{2}$$

where ρ is the density of the liquid, ω is the angular velocity of the CD platform, $\bar{R}$ is equal to $(R_1+R_2)/2$, and R_1 and R_2 are the two distances of the liquid elements from the center of the CD, as shown in Fig. 4(a). The burst frequency is defined as the angular frequency at which ΔP_c is

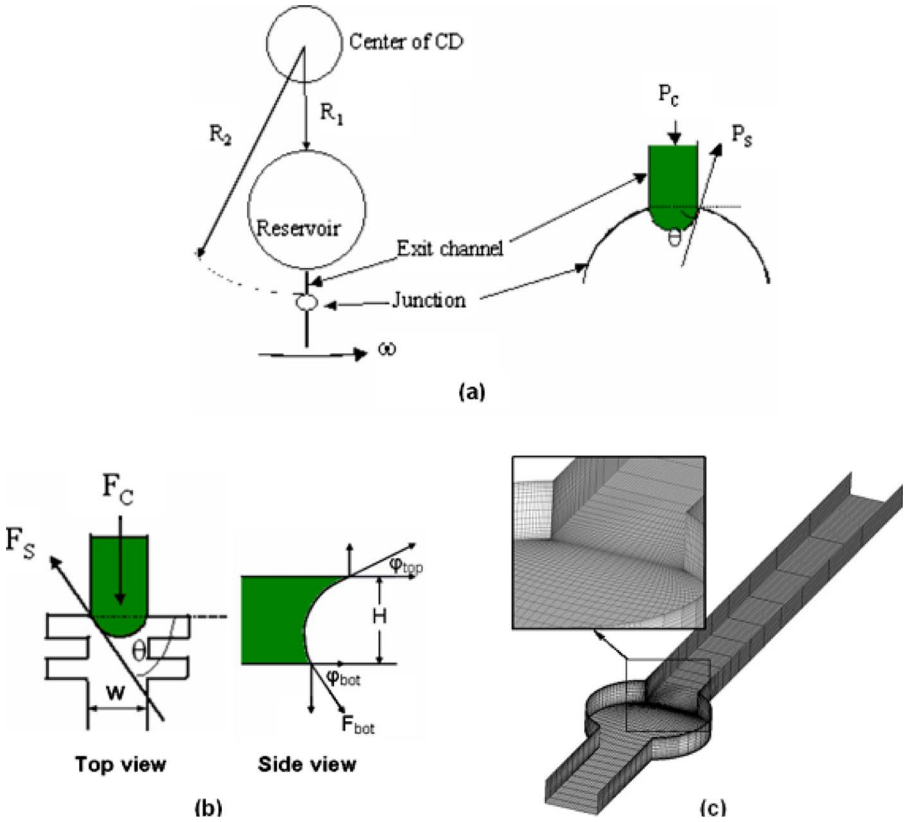

FIG. 4. Schematic of (a) a capillary valve with balance of centrifugal force and capillary force, (b) a fish-bone valve, and (c) computational mesh for capillary value.

greater than or equal to ΔP_s. At this rotation speed, the liquid overcomes the pressure generated by the capillary force and flows through the capillary valve, releasing liquid from the reservoir. The burst frequency f_b calculated from Eqs. (1) and (2) is given by

$$f_b = \left(\frac{\gamma \sin \theta}{\pi^2 \rho \cdot \Delta R \cdot \bar{R} \cdot d_H} \right)^{1/2}, \tag{3}$$

where d_H (equal to $4A/C$) is the hydrodynamic diameter of the channel connected to the junction. The capillary burst valve is a passive valve that requires no moving parts. It is controlled by the angular speed of rotation, fluid density, surface tension, and geometry and location of the channels and reservoirs. Flow sequencing was demonstrated in our previous work based on pure water,[6] indicating that good flow control can be obtained with the microchannels and reservoirs designed on the CD. Because of the characteristics of laminar flow inside the microfluidic channels, the solution filled in the optode reservoir can be physically and completely displaced by the subsequent incoming solution.

If contact angles on different surfaces are considered, the following equation derived from our previous work can be used to calculate the burst frequency:[30]

$$f_b = \sqrt{\frac{\gamma}{4\pi^2 \rho \cdot \Delta R \cdot \bar{R}} \left(\frac{2 \sin \theta}{W} - \frac{\cos \varphi_{\text{top}}}{H} - \frac{\cos \varphi_{\text{bot}}}{H} \right)}, \tag{4}$$

where W and H are the channel width and depth, respectively, θ is the contact angle from the top view, and φ_{top} and φ_{bot} are the contact angles of the lid and the bottom of the channel from the side view, respectively [shown in Fig. 4(b)].

The burst frequencies for all valves are also numerically predicted using the commercial CFD code FLUENT 6.3. In order to reduce the mesh size, the effect of circular reservoir is not considered and only the valve and the straight channel connecting the reservoir and valve are simulated. This simplification is reasonable because the centrifugal force applied on the liquid in the reservoir only depends on the radius coordinate and not on width or depth of the channel. The whole computational domain is discretized with 58 200 structured hexahedral meshes. Grid density is increased in the area of the waterfront position. Figure 4(c) shows the computational domain and the mesh scheme. The rotating movement of the channel is simulated by the rotating multiple reference frame (MRF) model in FLUENT. The centrifugal force was added automatically as a source term in the governing equations for the rotating MRF. The liquid-air interface was predicted using the volume of fluid model. The volume fractions of the liquid and the air were tracked throughout the domain during the computation. Also the interface between the liquid and air is defined at the position where the volume fraction of either liquid or air equals to 0.5. The inlet and outlet of the domain were assumed as atmospheric pressure. All the walls are nonslip and the contact angle was specified based on experimental conditions. Measured valve dimensions are used in the simulation. The rotation speed for a valve is initially set to 50 rpm and then increased in steps with an increment of 50 rpm. When the rotation speed is less than the burst frequency, the calculated will show fluctuations and eventually converge to zero due to the balancing between the centrifugal force and the capillary force. After reaching the burst frequency, i.e., after N computation steps, the flow rate will suddenly be a constant value and not drop to zero. This means that the liquid has burst into the valve. Therefore, the burst frequency of this valve is between $50(N-1)$ rpm and $50N$ rpm. The smaller the increment, the more accurate the burst frequency can be predicted; however, more computation time will be required.

D. Surface modification in the valve areas via polyaniline nanofibers

To make the valve surface superhydrophobic and much less affected by protein binding, polyaniline nanofibers, along with the noncrystalline fluorine coating (CYTOP 805A, Asahi Glass Co., Ltd.), were used to create nanostructures on the capillary valves by the solvent casting method. Polyaniline nanofibers were prepared using the dilute polymerization as described in our previous publication.[43] First, aniline was dissolved in a small portion of 1 M dopant acid solution and carefully transferred to the solution of APS dissolved in 1 M dopant acid solution. In the reaction mixture the initial concentration of aniline to the total volume of solution was maintained at $0.1M$, and the molar ratio of aniline to APS was kept at 1.5 for all syntheses. The reaction was carried out at room temperature with no disturbance. After 1 h, the dark-green precipitate of polyaniline nanofibers was collected to the centrifuge tube and then purified with DI water until the pH of the supernatant became ~ 5 using high-speed centrifuge at 5000 rmp at 23 °C. After decanting the final supernatant ($\sim p\mathrm{H}=5$), one volume of the concentrated polyaniline nanofiber suspension was diluted using two volumes of water before use. Dilute polyaniline nanofiber suspension was micropipetted into the capillary valve areas and after air drying for 2 h, the CYTOP 805A solutions with 1.0–6.0 wt % concentration were then dropped on the polyaniline treated PMMA surface and immediately dried by compressed air, achieving superhydrophobicity. The modified surface was characterized by using contact angle measurement and scanning electron microscopy (SEM). The capillary valves with modified surface were also evaluated by carrying out the flow sequencing testing after protein blocking.

E. Contact angle measurement

To examine the surface hydrophobicity, DI water was micropipetted on various surfaces (PMMA flat, CYTOP-treated flat, and CYTOP-polyaniline-treated surface) at room temperature and the diameter of the pipette tip was around 1.0 mm. After a COHU high-performance charge-coupled device (CCD) camera (1.27 cm view area) captured the water drop profile on the surface, software programs such as ADOBE PHOTOSHOP and UTHSCSA IMAGE TOOL were used to edit the pictures. The contact angle was obtained by measuring the sessile drop profile analyzed with a

MATLAB code. To evaluate the effect of protein blocking, the flat modified PMMA samples were immersed in 1.0% BSA solution for 10 min and then air dried for contact angle measurement.

F. Scanning electron microscopy

To visually examine the surface and interior morphology of modified surface, a Hitachi Model S-4300 SEM was used to analyze the nanostructure. The air-dried samples were loaded on the surface of an aluminum SEM specimen holder and sputter coated with gold for 2 min (Pelco Model 3 Sputter Coater) before observation. A working distance of about 10–20 mm, an accelerating voltage of 10 kV, and a chamber pressure of 10^{-8} Torr were found to be suitable for obtaining high-resolution images of samples. The magnification used in this study varied from 2000× to 120 000× depending on the nanostructures.

G. Protein blocking

After CD chips were injection-molded and the channel/reservoir surface was modified, cover lids need to be added to close the flow channels and reservoirs. The compact disk can be bonded together by the CO_2-assisted bonding[44] without losing the bioactivity of preloaded reagents. Before bonding, the lid was aligned with the patterned chip and stacked between two aluminum plates. The whole assembly was then placed inside the pressure vessel. After saturation with low pressure CO_2 (1.7 MPa) at 37 °C and pressure for 0.5 h, the pressure was quickly released and the chips were taken out of the vessel to evaluate the valve function and flow sequencing testing. Before testing, 1.0 wt % BSA blocking solution was introduced into microchannels for 10 min. Then the solution was removed by vacuum and the channel was rinsed by DI water three times, followed by vacuum drying. Finally, a 0.2 wt % BSA solution in DI water colored by food dye was introduced into the sample reservoir. Channels without BSA blocking were used as the control.

H. Valving testing

The disk was mounted on a motor plate (up to 4000 rpm) designed by Gamera Bioscience. The motor control was constructed of a five-stage stepper motor, a 12 V power supply, and a controller (PIC-Servo, HdB Electronics, Redwood City, CA). The motor was controlled directly via an RS232 serial port connection to a desktop PC, allowing integrated software control. The rotation speed of the disk was gradually increased until the release of fluid from the reservoir occurred. The motor was connected to an encoder to trigger a strobe (Monarch, DA 115/Nova Strobe) for synchronized imaging. The experiment repeated three times and the data represented the mean ± standard deviation (SD).

I. Immobilization of antibody through oxygen-PEI-TR-catalyzed reaction

Because only the detection area was treated with an oxygen-PEI-TR-catalyzed reaction, the other areas on PMMA chips were covered by aluminum foil before treatment. The oxygen-plasma treatment was carried out at 13.56 MHz using a bench top reactive ion etching system (Technics 800II RIE system). Before use, the plasma chamber was cleaned with 2-propanol, dried, and further cleaned using a 20 SCCM (SCCM denotes cubic centimeter per minute at STP) oxygen plasma at 200 W for 5 min. PMMA CD-ELISA chips were then placed near the center of the chamber, followed by evacuation to a base pressure of 12 mTorr. Oxygen gas was then introduced at a flow rate of 20 SCCM and the glow discharge was ignited at 300 W. After 30 s, the power and oxygen were turned off and the chamber was evacuated to 12 mTorr again. The chamber was then purged and the samples were taken out. The PMMA chips pretreated by oxygen plasma were immediately immersed into 0.2% PEI solution with pH=11.5 at room temperature to get the aminated PMMA samples. After 60 min, these aminated PMMA samples were directly applied for protein A immobilization using TR-catalyzed reaction. Briefly, TR solution was added to protein A solution and then incubated in the solution mixture at 4 °C for 4–12 h. The amount of TR added,

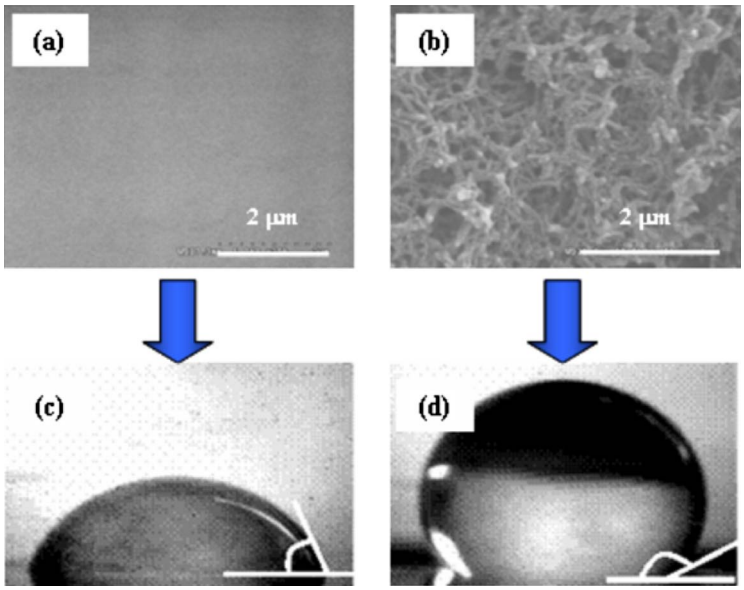

FIG. 5. SEM images of (a) a PMMA surface and (b) a CYTOP-polyaniline nanofiber-coated PMMA surface, and the water contact angles on the surface with different treatments before BSA blocking: (c) PMMA and (d) CYTOPpolyaniline-coated PMMA.

the concentration of protein A, and the incubation time were optimized according to the ELISA fluorescence signal.[45] After reaction, the covered aluminum foil was removed and the PMMA plates were washed twice with 1×Phosphate buffered saline (PBS) buffer to remove unreacted protein A. As a comparison, the PMMA chips treated only by oxygen-plasma and plasma-PEI approaches were used to measure ELISA fluorescence signal.

J. ELISA in 96-well microtiter plates

ELISA in 96-well microtiter plate was performed according to the kits with minor modification. Before detection, the borate buffer solution, blocking solution, washing solution, and substrate solution were prepared. The substrate solution was prepared by dissolving 15 mg HPPA in 5 ml tris-HCl buffer (0.15 M, *p*H=8.5). Prior to use, 1 μl of 30% hydrogen peroxide was added in the HPPA solution and mixed thoroughly. Primary antibody (1 μg/ml, 100 μl/well), blocking solution (200 μl/well), biotinylated huIFN-γ detection mAb (1 μg/ml, 50 μl/well), IFN-γ (50 μl/well) and HRP-conjugated streptavidin solution (1:4000, 100 μl/well) were loaded into the 96 wells in sequence. The primary antibody was coated at 4 °C overnight. The blocking process was performed for 2 h at room temperature. A mixed solution of biotinylated huIFN-γ detection mAb and recombinant huIFN-γ cytokine antigen, and HRP conjugated streptavidin were incubated in wells for 2 h and 30 min, respectively. The wells were washed five and four times after antigen and incubation, respectively. The reaction was detected by a TECAN GENios plate reader. The experiment was repeated three times and the data represented the mean ± SD.

K. ELISA on the compact disk

Unless otherwise noticed, antigen, second antibody (1 μg/ml) solutions, washing solution, conjugate solution, and substrate solution were loaded into the corresponding reservoirs on the bond chips in sequence. Then the controllable motor drove the solutions in the reservoirs to pass the detection areas in sequence, where primary antibody and blocking agents have been preloaded. The rotation speed of the disk was gradually increased until the release of fluid from the reservoir occurred. Detection was carried out using the fluorescence microscope (Nikon Eclipse TE2000-U).

TABLE I. Water contact angle on PMMA surface with different treatments.

Surface	Protein blocking	Contact angle (deg)
PMMA	No	70
	Yes	40
CYTOP-PMMA	No	120
	Yes	93
CYTOP-polyaniline-PMMA	No	170
	Yes	165

III. RESULTS AND DISCUSSION

A. Comparison of capillary valves w/o surface treatment

Protein blocking changes the hydrophobicity of the microfluidic chip surface, leading to loss of valve function. Therefore, CYTOP-coated polyaniline nanofibers were used to modify the valve area. Figure 5 compares the water contact angles and the SEM photographs on the different modified surfaces. As can been seen, the contact angle on PMMA (the plastic used to make the CD chip) without any treatment is around 70°, which greatly decreases to 40° after protein blocking (shown in Table I). This clearly illustrates why the conventional capillary valve would fail after protein blocking. After CYTOP 805A treatment, the contact angles of PMMA before and after protein blocking are 120° and 93°. In contrast, The CYTOP 805A-polyaniline nanofiber treated surface [i.e., the superhydrophobic surface clearly seen from the image in Fig. 5(d)] maintains its superhydrophobic property after protein blocking with only a small contact angle decrease from 170° to 165°. This is due to the porous nanostructure on the surface. The wettability of the solid surfaces depends on both the surface roughness and the surface energy. The nanofiber coating increases the surface roughness [shown in Fig. 5(b)] and the CYTOP coating lowers the surface energy, allowing the surface to exhibit superhydrophobic properties. Because it is difficult for protein molecules in the blocking solution to bind onto the CYTOP-coated nanostructures, the contact angle changes a little after protein blocking.

The snapshots shown in Fig. 6 visually compare the valve performance with different surface treatments. Before the testing, BSA solutions were added to block all the remaining binding sites to eliminate the nonspecific binding. As can be seen, the CYTOP treated and CYTOP-polyaniline-treated capillary valves can hold the protein solution as opposed to the unmodified valve. Because

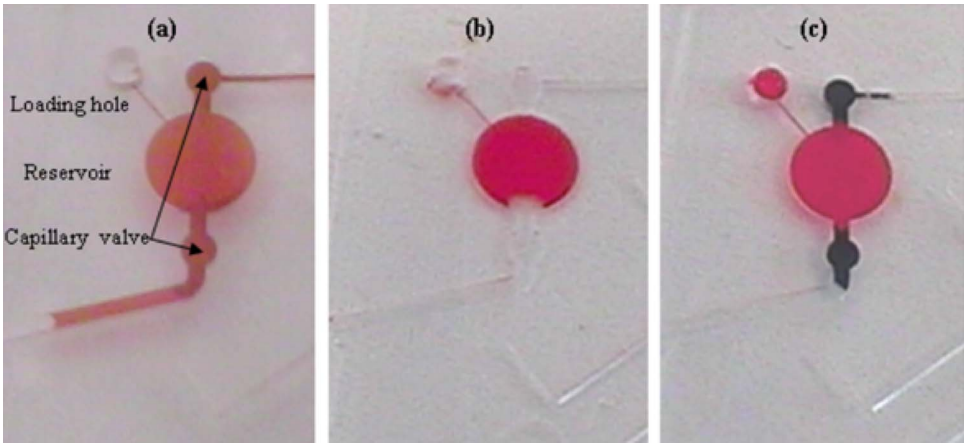

FIG. 6. (a) A capillary valve without any treatment cannot stop the mixed solution containing 0.1 wt % BSA and 1 wt % food dye after protein blocking. Also with (b) CYTOP or (c) CYTOP-polyaniline treatment, the capillary valve can hold the mixed solution.

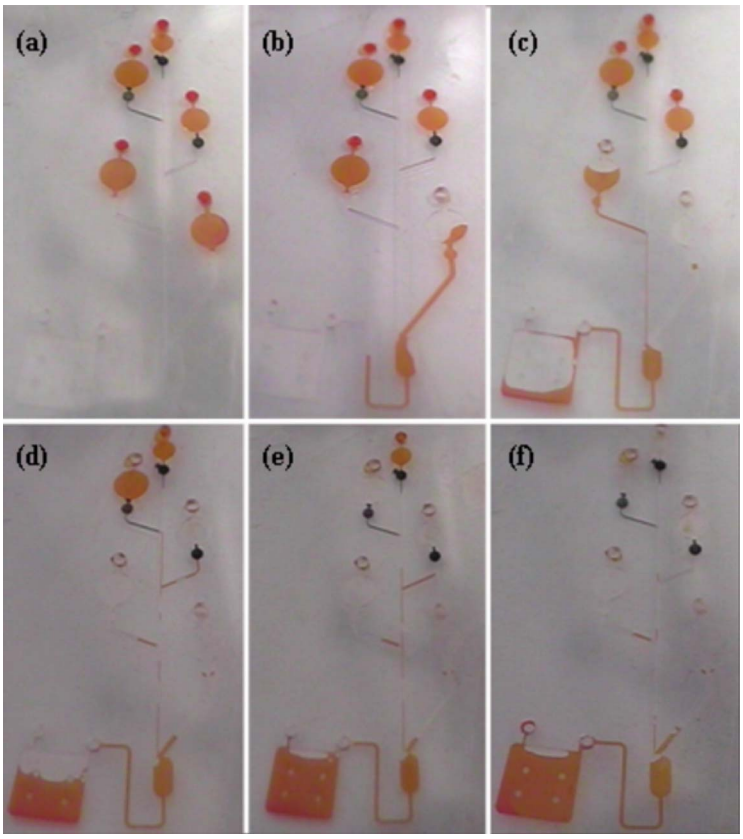

FIG. 7. Snapshots of the flow sequencing on a five-well CD chip with capillary valves: (a) Beginning, (b) 320 rpm, (c) 550 rpm, (d) 990 rpm, (e) 1220 rpm, and (f) 1600 rpm. Here, the capillary valves 1 and 2 were coated with CYTOP. Also the capillary valves 3–5 were treated with the CYTOP-polyaniline method.

the CYTOP-polyaniline treatment provides superhydrophobic property, a longer holding time for the reagents/washing solution in reservoirs can be achieved using this treatment than only CYTOP modification during the ELISA process (i.e., 530 rpm versus 327 rpm for a capillary valve treated with CYTOP-polyaniline and CYTOP, respectively). Compared with other superhydrophobic coating methods,[46] the polyaniline nanofibers can be easily applied onto microscale chips and provide a more consistent and reproducible surface modification.

B. Flow sequencing testing on PMMA disk

In order to test the burst frequency of each reservoir, protein blocking was carried out on the polyaniline-treated PMMA disks first. After being vacuum dried for 2 h, DI water containing red food dye was used as the test fluid and filled into different reservoirs. Their releases from different reservoirs were visualized and recorded by a CCD camera. The burst frequency was determined when each burst valve releases its solution. Burst frequencies of the reservoirs were designed to release at rotation speeds of ~200 rpm greater than the preceding reservoir. Figure 7 shows a series of snapshots taking during a test run. At a low rotation speed (327 rpm), only the fluid in reservoir 1 went to the waste reservoir, while the other fluids stayed in their reservoirs. When the rotation speed increased in steps, the fluids of wash 1, conjugate, wash 2, and the substrate moved to the waste reservoir in the right order.

Table II summarizes the channel dimensions and burst frequencies obtained from experiments and calculated from equations and numerical simulation. It is noted from the experimental data that the separations of burst frequencies are large enough to provide the desired fluid control. For example, the worst case of burst frequency separation in the experiment occurred between reser-

TABLE II. Dimensions and burst frequencies on the five-well CD chip. (Note: The designed channel depth is 200 μm and the actual depths for valves 1–5 are 157, 147, 161, 162, and 163 μm, respectively.)

No.	R_1 (mm)	R_2 (mm)	Channel width (μm)	Experimental f_b (rpm)	f_b from Eq. (3) (rpm)	f_b from Eq. (4) (rpm)	Simulated f_b using CFD code (rpm)
1	39.46	43.57	426 (450[a])	327 ± 25	819	331	350–400
2	34.50	38.52	232 (250[a])	546 ± 40	986	539	550–600
3	29.53	33.03	208 (225[a])	968 ± 16	584	898	750–800
4	24.53	28.42	92 (100[a])	1180 ± 45	739	1257	1000–1050
5	21.59	24.54	92 (100[a])	1506 ± 62	939	1600	1350–1400

[a]Designed value; experimental data are based on three CD chips.

voirs 3 and 4 (151 rpm). The calculated values based on Eq. (3) do not fit the experimental data well and even the flow sequencing has an incorrect order. In Eq. (3), it is assumed that all surfaces of the channel have the same contact angle and the channel is equivalent to a hydrodynamic cylinder. These assumptions are not realistic compared to the actual condition and geometry of the channel. Using Eq. (4) and the FLUENT simulation, the obtained burst frequencies fit the experimental data well. The simulation approach can be used to investigate the effect of contact angle on burst frequency (Table III) and to offer the three-dimensional information about the liquid-air interfaces shown in Figs. 8(a)–8(e). The shape of the interface is determined by the contact lines on four edges and the curvature of the surface. According to these figures, the two-side contact lines are locked at the edges where the straight channel connects to the valve. The top contact line is nearly a hemicycle while the bottom contact line depends on the surface properties of the valves. For a hydrophobic surface with a contact angle of 93° (valves 1 and 2), the surface curvature is positive in the horizontal direction but negative in the vertical direction, while on the superhydrophobic surface (valves 3–5), the curvatures in both directions are positive and have a larger value in the vertical direction.

Equation (4) and the FLUENT simulation approach involve controllable variables such as the channel dimensions, distances of the liquid elements from the center of the CD, and contact angles on the surfaces. By tuning these variables, the proper burst frequencies with a broader range could be predicted and achieved, which facilitates and directs the microdevice design.

C. Splitter performance on the compact disk

To increase the detection throughput, a splitter with a pair of sample reservoirs was employed in the microfluidic chips. To demonstrate whether the reagents loaded in the reservoirs can flow through the splitter equally, a red dye solution was filled in reservoirs 1, 1′, and 2. Figure 9 shows the snapshot when the rotation speed was set at 550 rpm. As can be seen, the red solution flowed through the splitters and reached the waste reservoirs. All the detection areas were filled with the red solution, indicating sufficient quantity of antigen to be captured. Therefore, this biochip with splitters has the capability to analyze 24 samples in duplicate providing 48-sample assay analysis.

TABLE III. Effect of contact angle on burst frequency for the no. 1 valve. (Note: Experimental data are based on three CD chips; measured dimensions are used as the input for simulation.)

Contact angle (deg)	Experimental f_b (rpm)	Simulated f_b using CFD code (rpm)
70	243 ± 27	250–275
93	327 ± 25	350–400
165	530 ± 35	475–500

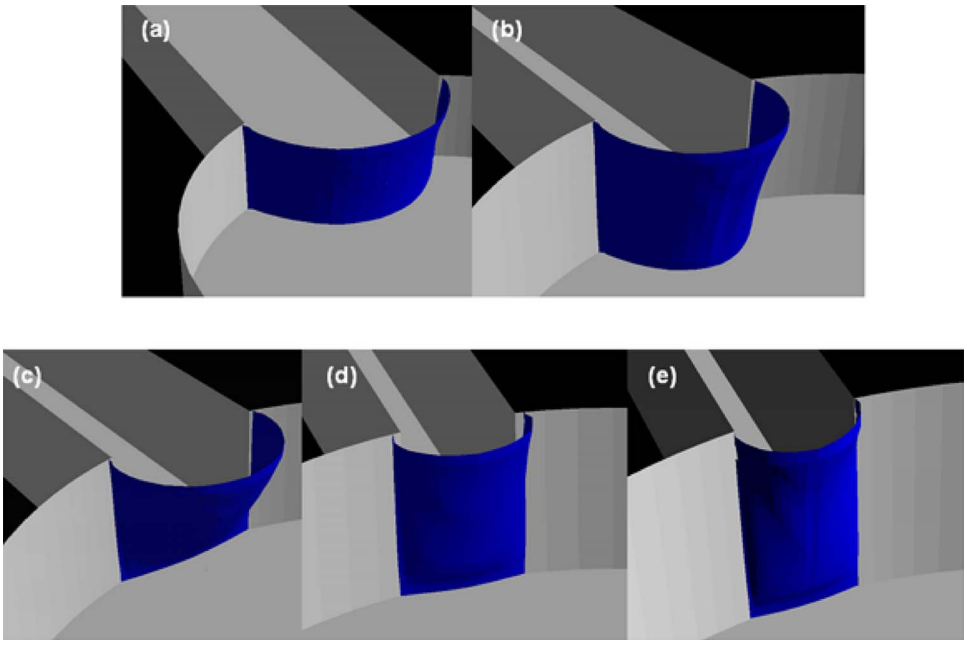

FIG. 8. Simulated liquid-air interfaces for capillary valves with different contact angles: (a) No. 1, 93° at 350 rpm; (b) No. 2, 93° at 550 rpm; (c) No. 3, 165° at 750 rpm; (d) No. 4, 165° at 1000 rpm; and (e) No. 5, 165° at 1350 rpm.

D. Comparison of ELISA performance with different antibody immobilization methods

Highly efficient antibody immobilization is extremely crucial for the enhancement of the sensitivity of ELISA immunoassay on CD. To achieve this, a site-selective TR-catalyzed protein A antibody immobilization technique was successfully developed in this study. To effectively immobilize the target antibodies, oxygen plasma was first used to activate the inert PMMA. This is followed by PEI coating, an amine-containing functional polymer. From ELISA detection signals shown in Fig. 10, the fluorescence intensity on untreated PMMA microchannel was only 2.61. It increased to 4.47 after modified only by PEI. When the PMMA microchannel was pretreated by oxygen plasma prior to PEI coating, the intensity increased to 13.80. Apparently more PEI was attached to the oxygen plasma treated PMMA surface resulting in higher amount of antibody binding and the final immunoreaction bioactivity. Figure 10 also shows that the enzyme reaction

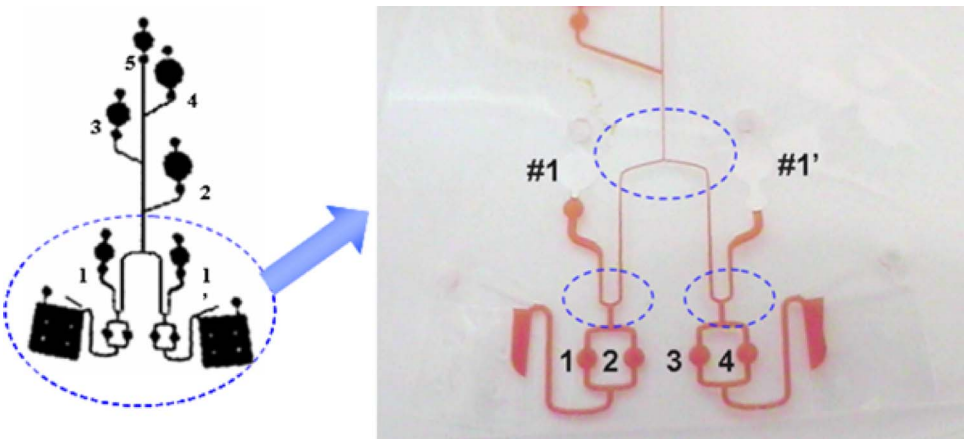

FIG. 9. Flow pattern demonstration carried out on a CD chip with the splitters.

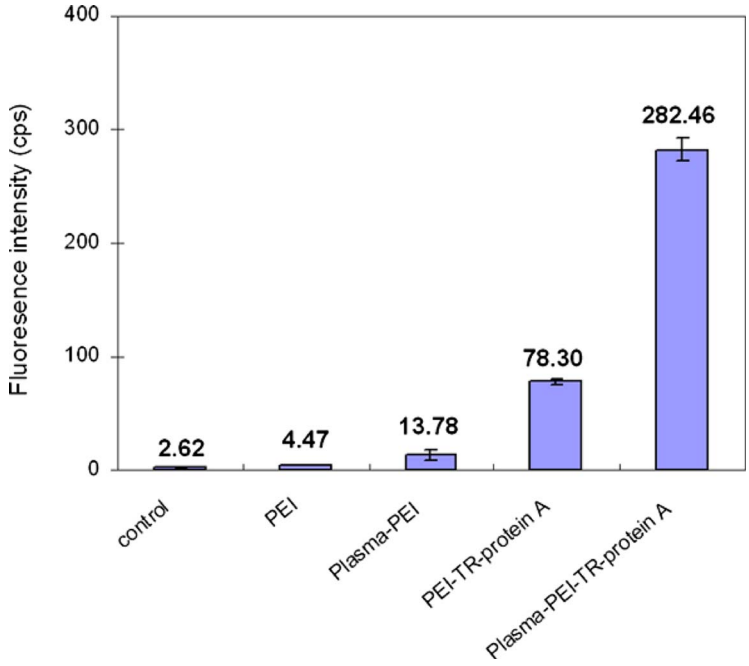

FIG. 10. Comparison of bioactivity of antibodies on microchips immobilized with different approaches. The averages and error bars were calculated from three independent samples.

is further increased when anti-IFN-γ was immobilized by protein A. This is particularly the case when protein A was immobilized via TR-catalyzed reaction (282.46), almost 62-fold increasing compared with the commonly used PEI surface modification method. It is reasonable to believe that this is due to the synergistic action of oxygen plasma treatment and TR-catalyzed chemistry. Oxygen plasma treatment can facilitate the PEI and antibody attachment. On the other hand, TR can specifically convert tyrosine histidine tags of protein A into O quinones, which in turn are highly reactive toward primary amines, resulting in the site-selective immobilization of the protein A receptor and the preservation of its high ligand affinity on the solid supports. As a result, protein A with ideal orientation can selectively immobilize the Fc regions of IgG through Fc-domain tags, leading to a high capture capacity of bound antibodies toward antigens. Moreover, this resulting oxygen plasma-PEI-TR-catalyzed protein A structure, especially on the surface with homogeneous nanometer-sized feature after plasma treatment, may serve as an extended matrix or a long spacer for antibody immobilization, allowing the anchored antibody to stay away from the solid substrate with an increased immunoreactive affinity to antigens.

E. Comparison of ELISA on the compact disk and in 96-well microtiter plate

ELISA detection of IFN-γ was carried out in both 96-well microtiter plates and microchips modified by the polyaniline nanofibers and an oxygen plasma-PEI-TR protein A surface treatment to compare their performance. The same concentrations of primary and second antibodies were used in the study, although larger total amounts (liquid volumes 5 μl versus 100 μl) were used for the 96-well plates. Figure 11 compares the ELISA results, where Figs. 11(a) and 11(b) correspond to 96-well microtiter plates and PMMA CD chips, respectively.

As shown in Fig. 11(a), a linear relationship between the fluorescence signal and the antigen concentration was observed from 0 to 1250 pg/ml in the 96-well microtiter plate. The fluorescence signal did not increase linearly at concentrations higher than 1250 pg/ml. The fluorescence intensity was proportional to the reaction time up to 10 min and became unchanged, suggesting that the enzyme reaction has reached the equilibrium. Therefore, the time required for stable fluorescence values marked in Fig. 11(a) is around 10 min. The fluorescence intensity was also linearly in-

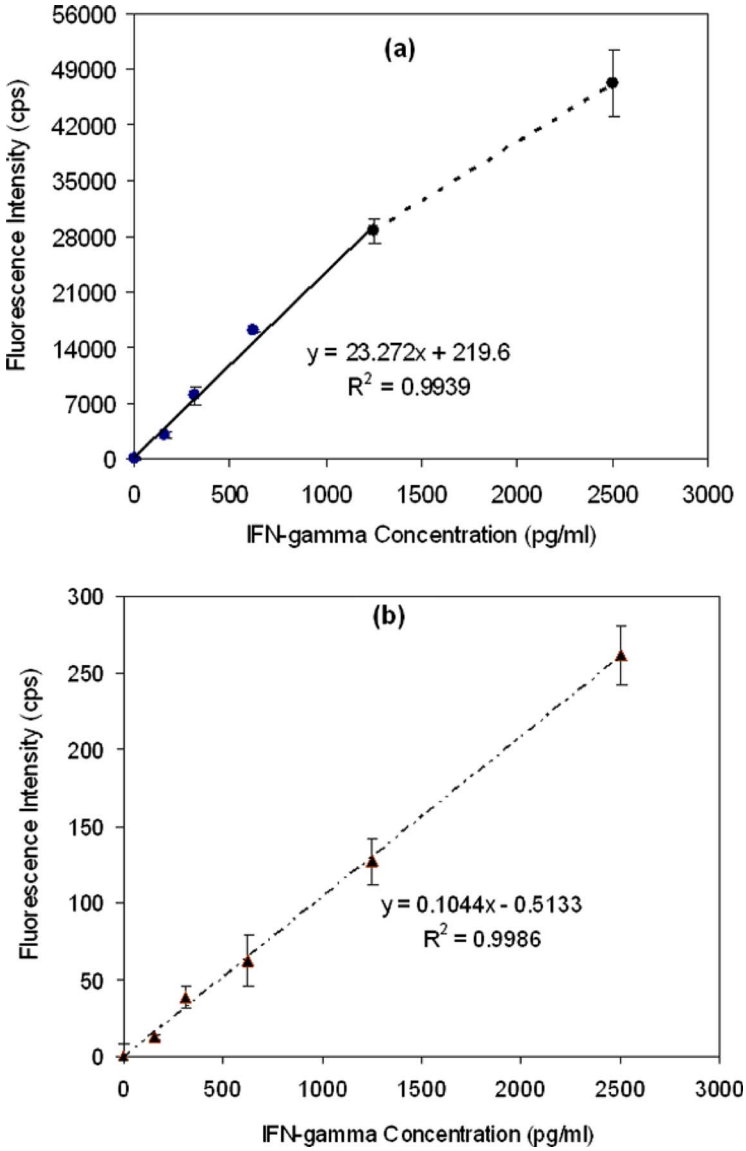

FIG. 11. Calibration curves for IFN-γ ELISA detection carried out (a) in a 96-well plate and (b) on a PMMA CD-like chip modified by the plasma-PEI-TR protein A method. The averages and error bars were calculated from three independent samples.

creased with the antigen concentration from 0 to 2500 pg/ml on a compact disk. The time required for stable fluorescence values decreased to 30 s for PMMA chips after modified by the proposed TR-catalyzed protein A method. This effect is attributed to an increase in the specific interfacial area, a reduction in diffusion length compared to 96-well microtiter plate, leading to a faster enzymatic reaction. The antibody immobilized via TR-catalyzed protein A in microchannel can provide better antigen capture capacity, directly resulting in the improvement of subsequent second antibody and enzyme binding efficiency. The CD-ELISA system described in this study represents an innovative approach to greatly simplify the process of cytokine analysis. Table IV summarizes the reagents used and incubation time in 96-well plates and microchips. As can be seen, a reaction volume was smaller by orders of magnitude and assay time was superior by an order of magnitude compared to the usual microtiter 96-well plate ELISA. This platform technology has advantages, including minimized reagent consumption and high-speed assay, and holds the potential for medical/pharmaceutical research and clinical testing.

TABLE IV. Comparison of 96-well plate and microchannels for IFN-γ detection.

	Reagent volume (μl)		Incubation time (min)	
Procedure	96-well plate	Microchip	96-well plate	Microchip
Coating	100	10	480	30
Blocking	200	10	120	15
IgG/sample	50	5	60	15
Second antibody	50	5	60	15
HRP conjugate	100	5	30	10
HPPA	100	5	30	1
Total	600	40	780	86

IV. CONCLUSION

In this study, a polymeric microfluidic biochip was designed and fabricated for ELISA based on the integration of a centrifugal fluidic platform and several surface treatment methods: Polyaniline nanofiber-modified capillary valving and the oxygen plasma-PEI-TR-protein A modification in the detection area. The proper flow sequencing was achieved on a CD-like microfluidic chip by using the capillary valves treated with polyaniline-based surface modification. The burst frequency for each valve was determined by experiments and can be calculated by a derived equation and a finite element code. This microfluidic biochip was successfully applied to the detection of a cytokine IFN-γ and can be used for immunoassay applications.

ACKNOWLEDGMENTS

This work is funded by the National Science Foundation sponsored Nanoscale Science and Engineering Center for Affordable Nanoengineering of Polymeric Biomedical Devices (NSEC-CANPBD) at The Ohio State University.

[1] L. F. Erdile, D. Smith, and D. Berd, J. Immunol. Methods **258**, 47 (2001).
[2] A. Meenakshi, R. S. Kumar, and N. S. Kumar, J. Immunoassay Immunochem. **23**, 293 (2002).
[3] S. Sirivichayakul, P. Phanuphak, S. Tanprasert, S. Thanomchat, C. Uneklabh, T. Phutiprawan, C. Mungklavirat, and Y. Panjurai, J. Clin. Microbiol. **31**, 1373 (1993).
[4] Y. Jeong, K. J. Kim, D. J. Kim, S. W. Oh, and E. Y. Choi, Clin. Chem. **49**, 826 (2003).
[5] J. S. Rossier and H. H. Girault, Lab Chip **1**, 153 (2001).
[6] S. Lai, S. Wang, J. Luo, L. J. Lee, S.-T. Yand, and M. J. Madou, Anal. Chem. **76**, 1832 (2004).
[7] J. Rossier and H. Girault, Lab Chip **1**, 153 (2001).
[8] K. Sato, M. Tokeshi, T. Odake, H. Kimura, T. Ooi, M. Nakao, and T. Kitamori, Anal. Chem. **72**, 1144 (2000).
[9] K. Sato, M. Tokeshi, H. Kimura, and T. Kitamori, Anal. Chem. **73**, 1213 (2001).
[10] N. G. Anderson, Science **166**, 317 (1969).
[11] C. D. Scott and C. A. Burtis, Anal. Chem. **45**, 327A (1973).
[12] T. O. Tiffany, C. A. Burtis, and N. G. Anderson, Methods Enzymol. **31**, 790 (1974).
[13] T. Klumpp, Ann. Biol. Clin. **35**, 221 (1977).
[14] V. Henry, J. Deutsch, and G. Lum, Clin. Chem. **24**, 514 (1978).
[15] M. Madou, L. J. Lee, S. Daunert, S. Lai, and C.-H. Shih, Biomed. Microdevices **3**, 245 (2001).
[16] http://www.gyros.com/en/products/gyrolab_workstation/
[17] R. H. Liu, Q. Yu, J. M. Bauer, J. S. Moore, and D. J. Beebe, in *Technical Digest of Solid-State Sensor & Actuator Workshop*, Hilton Head Island, SC, June 2000, pp. 222–226.
[18] X. Cao, S. Lai, and L. J. Lee, Biomed. Microdevices **3**, 109 (2001).
[19] P. Griss, H. Andersson, and G. Stemme, Lab Chip **2**, 117 (2002).
[20] M. A. Unger, H. P. Chou, T. Thorsen, A. Scherer, and S. R. Quake, Science **288**, 113 (2000).
[21] S. Z. Hua, F. Sachs, D. X. Yang, and H. D. Chopra, Anal. Chem. **74**, 6392 (2002).
[22] D. C. Duffy, H. L. Gills, J. Lin, N. F. Sheppard, and G. Kellogg, Anal. Chem. **71**, 4669 (1999).
[23] M. J. Madou, Y. Lu, S. Lai, L. J. Lee, and S. Daunert, Biomed. Microdev. **3**, 245 2001).
[24] H. Y. Erbil, A. L. Demirel, Y. Avci, and O. Mert, Science **299**, 1377 (2003).
[25] Q. Xie, J. Xu, L. Feng, W. Tang, X. Luo, and C. C. Han, Adv. Mater. (Weinheim, Ger.) **16**, 302 (2004).
[26] X. Lu, C. Zhang, and Y. Han, Macromol. Rapid Commun. **25**, 1606 (2004).
[27] L. Feng, Y. Song, J. Zhai, B. Liu, J. Xu, L. Jiang, and D. Zhu, Angew. Chem. **115**, 824 (2003).
[28] I. Woodward, W. C. E. Schofield, V. Roucoules, and J. P. S. Badyal, Langmuir **19**, 3432 (2003).

[29] T. Sun, G. Wang, L. Feng, B. Liu, Y. Ma, L. Jiang, and D. Zhu, Angew. Chem., Int. Ed. **43**, 357 (2004).
[30] C. Lu, Y. Xie, Y. Yang, M. M.-C. Cheng, C.-G. Koh, Y. Bai, L. J. Lee, and Y.-J. Juang, Anal. Chem. **79**, 994 (2007).
[31] M. Herrmann, E. Roy, T. Veres, and M. Tabrizian, Lab Chip **7**, 1546 (2007).
[32] K. Sato, M. Yamanaka, T. Hagino, M. Tokeshi, H. Kimura, and T. Kitamori, Lab Chip **4**, 570 (2004).
[33] M. Kakuta, H. Takahashi, S. Kazuno, K. Murayama, T. Ueno, and M. Tokeshi, Meas. Sci. Technol. **17**, 3189 (2006).
[34] L. Yu, C. M. Li, and Q. Zhou, Front. Biosci. **10**, 2848 (2005).
[35] Y. Jang, S. Y. Oh, and J.-K. Park, Enzyme Microb. Technol. **39**, 1122 (2006).
[36] T. G. Henares, S. Funano, S. Terabe, F. Mizutani, R. Sekizawa, and H. Hisamoto, Anal. Chim. Acta **589**, 173 (2007).
[37] Y. L. Bai, C. G. Koh, M. Boreman, Y. J. Juang, I. C. Tang, L. J. Lee, and S. T. Yang, Langmuir **22**, 9458 (2006).
[38] J. M. Fowler, M. C. Stuart, and D. K. Y. Wong, Anal. Chem. **79**, 350 (2007).
[39] A. A. Karyakin, G. V. Presnova, M. Y. Rubtsova, and A. M. Egorov, Anal. Chem. **72**, 3805 (2000).
[40] H. Wang, Y. L. Liu, Y. H. Yang, T. Deng, G. L. Shen, and R. Q. Yu, Anal. Biochem. **324**, 219 (2004).
[41] G. Y. Shen, H. Wang, T. Deng, G. L. Shen, and R. Q. Yu, Talanta **67**, 217 (2005).
[42] C. P. Johnson, I. E. Jensen, A. Prakasam, R. Vijayendran, and D. Leckband, Bioconjugate Chem. **14**, 974 (2003).
[43] N.-R. Chiou and A. J. Epstein, Adv. Mater. (Weinheim, Ger.) **17**, 1679 (2005).
[44] Y. Yang, C. Zeng, and L. J. Lee, Adv. Mater. (Weinheim, Ger.) **16**, 560 (2004).
[45] Y. Yuan, H. He, and L. J. Lee, Biotechnol. Bioeng. **102**, 891 (2009).
[46] P. van der Wal and U. Steiner, Soft Matter **3**, 426 (2007).